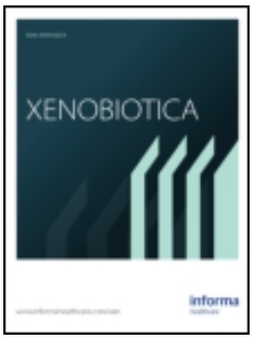

Taylor & Francis
Taylor & Francis Group

Xenobiotica
the fate of foreign compounds in biological systems

ISSN: 0049-8254 (Print) 1366-5928 (Online) Journal homepage: https://www.tandfonline.com/loi/ixen20

Evaluation of seven drug metabolisms and clearances by cryopreserved human primary hepatocytes cultivated in microfluidic biochips

Régis Baudoin, Jean Matthieu Prot, Grégory Nicolas, Jessy Brocheton, Céline Brochot, Cécile Legallais, Henri Benech & Eric Leclerc

To cite this article: Régis Baudoin, Jean Matthieu Prot, Grégory Nicolas, Jessy Brocheton, Céline Brochot, Cécile Legallais, Henri Benech & Eric Leclerc (2013) Evaluation of seven drug metabolisms and clearances by cryopreserved human primary hepatocytes cultivated in microfluidic biochips, Xenobiotica, 43:2, 140-152, DOI: 10.3109/00498254.2012.706725

To link to this article: https://doi.org/10.3109/00498254.2012.706725

Xenobiotica, 2013; 43(2): 140–152

ISSN 0049-8254 print/ISSN 1366-5928 online
DOI: 10.3109/00498254.2012.706725

informa
healthcare

RESEARCH ARTICLE

Evaluation of seven drug metabolisms and clearances by cryopreserved human primary hepatocytes cultivated in microfluidic biochips

Régis Baudoin[1], Jean Matthieu Prot[1], Grégory Nicolas[2], Jessy Brocheton[3], Céline Brochot[4], Cécile Legallais[1], Henri Benech[2], and Eric Leclerc[1]

[1]Laboratoire de Biomécanique et Bio ingénierie, CNRS UMR 7338, Université de Technologie de Compiègne, France, [2]CEA, Service de Pharmacologie et d'Immunoanalyse, DSV/iBiTec-S, CEA/Saclay, Gif-Sur-Yvette Cedex, France, [3]Plate-Forme Génomique, Institut Cochin, 22 rue Méchain, Paris, France, and [4]Institut National de l'Environnement Industriel et des Risques (INERIS), Unité Modèles pour l'Ecotoxicologie et la Toxicologie (METO), Parc Alata BP2, Verneuil-en-Halatte, France

Abstract

We present characterization of the metabolic performance of human cryopreserved hepatocytes cultivated in a platform of parallelized microfluidic biochips. The RTqPCR analysis revealed that the mRNA levels of the cytochromes P450 (CYP 1A2, 2B6, 2C8, 2C9, 2C19, 2D6, 2E1, 3A4) were reduced after the adhesion period (when compared to the post-thawing step). The microfluidic perfusion played a part in stabilizing and partially recovering the levels of the HNF4α, PXR, OAPT2, CYP 1A2, 2B6, 2C19 and 3A4 mRNA on contrary to non-perfused cultures. Fluorescein diacetate staining and P-gp mRNA level illustrated the hepatocytes' polarity in the biochips. Drug metabolism was assessed using midazolam, tolbutamide, caffeine, omeprazole, dextromethorphan, acetaminophen and repaglinide as probes. Metabolite detection and quantification revealed that CYP1A2 (via the detection of paraxanthine), CYP3A4 (via 1-OH-midazolam, and omeprazole sulfone detection), CYP2C8 (via hydroxyl-repaglinide detection), CYP2C19 (via hydroxy-omeprazole detection) and CYP2D6 (via dextrorphan detection) were functional in our microfluidic configurations. Furthermore, the RTqPCR analysis showed that the drugs acted as inductors leading to overexpression of mRNA levels when compared to post-thawing values (such as for HNF4α, PXR and CYP3A4 by dextromethorpahn and omeprazole). Finally, intrinsic *in vitro* biochip clearances were extracted using a PBPK model for predictions. The biochip predictions were compared to literature *in vitro* data and *in vivo* situations.

Keywords: Human cryopreserved hepatocytes, IDCCM, microfluidic biochips, drug metabolism, clearances

Introduction

There is now a widespread need to develop methods that are not based on *in vivo* animal testing (Greim et al. 2006; Blaauboer & Andersen 2007; Hartung & Rovida 2009). The priority for research is to develop alternative *in vitro* and *in silico* approaches and then link them together to produce methods that benefit from the complementary nature of the two (Bhogal et al. 2005). To refine cell-based assays, microscale bioartificial organs have been proposed using recent developments in the field of micro-technology to design *in vitro* systems on a very small scale. Among these microscale organs, specific developments on livers have been made to propose liver microfluidic biochips as a means of investigating drug and xenobiotic metabolisms or hepatotoxicity (Griffith & Naughton 2002; Powers et al. 2002; Sivaraman et al. 2005; Chao et al. 2009; Prot et al. 2011a; Novik et al. 2010; Baudoin et al. 2011, Zhang et al. 2011).

In a previous study using polydimethylsiloxane (PDMS) microfluidic biochips, we found that the Nrf2-dependent pathway (such as the AHR signalling pathway) in HepG2/C3a cell lines was upregulated in

Address for Correspondence: Eric Leclerc, aboratoire de Biomécanique et Bioingénierie, Université de Technologie de Compiègne, France. Tel: 33 (0)3 44 23 79 43. E-mail: eric.leclerc@utc.fr

(Received 10 May 2012; revised 20 June 2012; accepted 22 June 2012)

our microfluidic biochip cultures (Prot et al. 2011a, 2011b). Several hypotheses were proposed to explain this induction. The microfluidic culture was supposed to induce a global cytoprotective response leading to the induction of cell defence mechanisms, including drug metabolism. In addition, from our previous work using a microarray analysis, it was also shown that the HepG2/C3a cultivated in our microfluidic biochips presented a zonation-related pattern, whereas Petri cultures presented pronounced kinase signalling and cancer specific profiles (Cheng et al. 2012). Furthermore, based on metabolomics profiling and metabolic flux reconstruction, oxygenation and glycolysis homeostasis appeared to be enhanced in the biochips when compared to hepatic Petri cultures (Shintu et al. 2012; Ouattara et al. 2012). Combined with microfluidic perfusion in a PDMS material (highly oxygen permeable), hepatocyte hypoxia might be reduced leading to better maintenance of the cytochrome P450 (CYP) level. As high and efficient oxygenation is a key factor for functional hepatocytes, this result also played a part in explaining the level of CYP mRNA in the HepG2/C3a cultivated in biochips. Therefore, we found several parameters related to liver cell adaptation in our micro-environment which may lead to the xenobiotic metabolism pathways being triggered.

To complete the development of liver microfluidic biochips, we had to move from cell lines (HepG2/C3a) to primary hepatocytes. To do so, we extended our studies to evaluating metabolic performance using human cryopreserved primary hepatocytes (Prot et al. 2011c). Hepatocytes were exposed to the CIME cocktail (Carte d'Identité MEtabolique), a mixture of seven probes for key enzymes involved in xenobiotic metabolism and pharmacokinetics. The results showed greater activity for CYP1A2, CYP2C9, CYP2C19 CYP2D6, CYP3A and UGT1A1 after 4 h of incubation in the microfluidic biochip when compared to the plated cultures. Furthermore, the metabolic time-course ratio measured at 1 h, 3 h and 4 h indicated that enzymatic activity was higher when the hepatocytes were cultivated in the microfluidic biochips, in contrast with their response in the plated cultures. These first sets of results illustrate the functional relevance of liver cultures using human primary hepatocytes in our design and configuration of culture. However, given that we worked with a cocktail of molecules, we did not calculate metabolic clearance due to the lack of individual substrate data.

To be able to transfer this microfluidic methodology to industrial applications, we have developed a specific culture box for parallelized microfluidic cultures (Baudoin et al. 2011). The entire set up, named IDCCM for "Integrated Dynamic Cell Culture in Microfluidic biochips" makes possible the perfusion culture of 12 biochips simultaneously. Thanks to the hermetic cover and autoclave of the IDCCM box, we were able to perform long-term cell cultures in sterile conditions. The microfluidic cultures reproduce a dynamic micro-environment for cell cultures which is important for hepatocyte zonation and nutrient or xenobiotic disposition, as mentioned above.

The aim of this present article was to characterize and estimate the potential of the IDCCM box for drug clearance applications. To do so, we set up a culture of human cryopreserved hepatocytes in the microfluidic biochips of the IDCCM box. Then, we analyzed the mRNA levels related to xenobiotic metabolism when hepatocytes are cultivated in the biochips. In addition, we tested the metabolism of seven well-known drugs and hepatic substrates. Based on these data, we proposed the development of a kinetic model to describe the fate of the drugs. This led to the extraction of intrinsic hepatic clearances. Production of metabolites and non-specific binding was considered. Finally, we compared the results with those obtained in other biochips or conventional cultures presented in the literature.

Material and methods

IDCCM tool box and microfluidic biochips

The biochip design and microfabrication, as well as the key features and functionality of the IDCCM box, have been described previously (Baudoin et al. 2011; in press). Briefly, a polycarbonate box was manufactured using the conventional 24-well plate as a dimensional model for the box format. Each microfluidic biochip was connected between two wells in the box. The 24 wells were used as entrance and outlet reservoirs leading to the parallelization of 12 biochips (Figure 1). A specific cover was designed to make it possible to seal the polycarbonate box hermetically. The cover includes ports for fluid perfusion and sampling. The entire set-up has been named the IDCCM box (Integrated Dynamic Cell Culture in Microfluidic biochips"). The biochips were made from polydimethysiloxane (PDMS) using conventional replica molding.

Drugs

The following substrates and metabolites used to prepare the standard solutions were obtained from Sigma-Aldrich (St Quentin Fallavier, France): acetaminophen (APAP, CAS 103-90-2), acetaminophen glucuronide (APAP-GLU, CAS 120595-80-4), caffeine (CAF, CAS 58-08-2), paraxanthine (PARA, CAS 611-59-6), dextromethorphan (DEXTM, CAS 6700-34-1), dextorphan-D-tartrate (DEX, CAS 143-98-6), 3-methoxymorphinan hydrochloride (3-MM, CAS 36397-14-5), midazolam maleate salt (MDZ, CAS 59467-94-6), 1-OH midazolam (1OH-MDZ, CAS 59468-90-5), 4-OH midazolam (4OH-MDZ, CAS 59468-85-8), omeprazole (OME, CAS 73590-58-6), repaglinide (REP, CAS 135062-02-1) and tolbutamide (TOLB, CAS 64–77-7). 5-OH omeprazole (5OH-OME, CAS 92340-57-3) and 4-OH tolbutamide (4OH TOLB, CAS 5719-85-7) were obtained from SPI-Bio (Montigny Le Bretonneux, France). Omeprazole sulfone (OME-SULF, CAS 88546-55-8) was obtained from @rtMolecule (Poitiers, France).

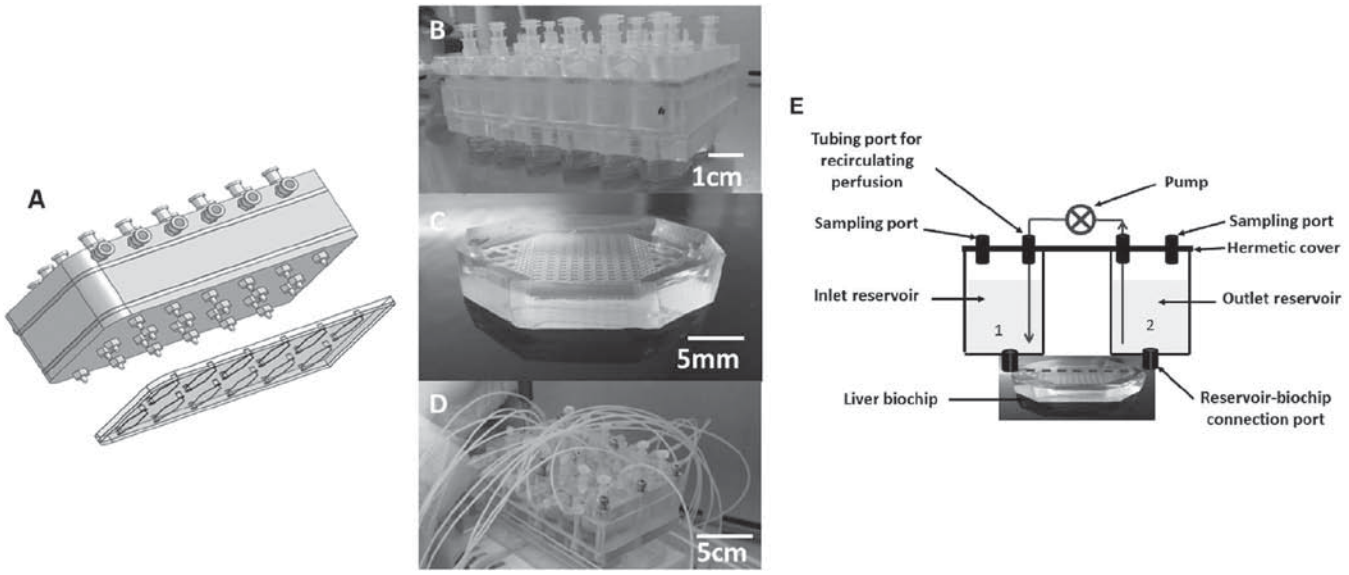

Figure 1. (A) Principle and design of the IDCCM box; (B) IDCCM box with connected biochips; (C) View of one biochip; (D) IDCCM box with PTFE tubes and loaded culture medium; (E) Schematic of a basic unit of the IDCCM box.

3-hydroxyrepaglinide (3OH-REP, CAS 874908-14-2) was obtained from TRC (Toronto, Canada).

Human hepatocyte preparation

Cyopreserved hepatocytes from two human donors (BioPredict, Rennes, France) were warmed at 37°C and pooled together in a 50 mL flask in 40 mL of warmed Leibowitz L15 medium. After a 50*g* centrifugation for 2 min, the cell pellet was suspended in a 28% percoll solution and centrifuged at 50*g* for 5 min. After removing the supernatant, viable cells were suspended in 2 mL of seeding medium. The seeding medium was a Williams E Glutamax medium supplemented with penicillin 100 UI/mL, streptomycin 100 µg/mL, bovine insulin 4 µg/mL and fetal calf serum 10% v/v. Viability was achieved by means of trypan blue exclusion and cell number was determined with a Malassez cell. After that, a final centrifugation at 50*g* for 4 min was performed in order to adjust the cell concentration to the desired inoculated cell density.

Dynamic culture in liver microfluidic biochips

The biochips were coated with collagen type I at 5 µg/cm^2 for 1 h and rinsed. The hepatocytes suspended in the seeding medium were inoculated into the liver biochip at $2 \pm 0.1 \times 10^5$ cells/cm^2 and placed without flow in a CO_2 incubator at 37°C for the adhesion period (24 h). After adhesion, the cells were rinsed and connected to the perfusion circuit made of PFTE tubes. The reservoir and the circuit were loaded with 3 mL of an incubation medium including the substrates at 1 µM. The incubation medium was a Williams E Glutamax medium supplemented with penicillin 100 UI/mL, streptomycin 100 µg/mL and bovine insulin 4 µg/mL. The incubation medium containing each substrate at 1 µM was incubated for 24 h and sampled after 1 h, 2 h, 3 h, 4 h, 5 h and 24 h. To do so, the peristaltic pump was started at a flow rate of 25 µL/min. All the sampled volumes were collected and diluted in acetonitrile (1/3). The samples were stored in Eppendorf tubes at –80°C until the LC-MS/MS analysis.

Cell counting and staining

Before inoculation, after adhesion, and at the end of the cultures, cells were counted using a Malassez cell. Viability was quantified by trypan blue staining. Calcein AM staining was used to perform *in situ* visualizations of living cells on the biochip. Fluorescein diacetate was used to illustrate the transcellular transports on the living cells at the end of the experiments.

Analysis

The analytical method has been presented in detail by Videau et al. (2010). Briefly, samples were evaporated to dryness using a Turbovap LV evaporator (Zymark, Roissy, France). The dry residue was reconstituted in 60 µL of 2 mM ammoniumacetate/methanol 9/1 v/v. After vortex mixing, 40 µL was injected into the chromatographic system. Detection and processing was performed using a Waters Acquity UPLC system coupled to a triple quadripole mass spectrometer Xevo TQ-MS equipped with an electrospray ionization source (Waters, Saint Quentin en Yvelines, France). System control and data processing were carried out using MassLynx software, version 4.1. Quantification was performed using the TargetLynx application.

The peak area of all the analytes was determined using a reversed phase UPLC method with tandem mass spectrometric detection according to a previously described assay (Videau et al. 2010). Samples were run on an ACQUITY UPLC® BEH Shield RP18 column (2.1 × 100 mm, 1.7 µm) coupled with an ACQUITY

UPLC® BEH Shield RP18 1.7 µm Van Guard® Pre-Column (Waters, St. Quentin en Yvelines, France). Mobile phases were delivered as a gradient of a first solvent composed of 0.1% formic acid in water and a second mobile phase solvent of 0.1% formic acid in acetonitrile. The flow rate was set at 0.4 mL/min and temperatures were 50°C and 4°C for the column and autosampler, respectively. Run time was 8 min.

The LC-MS/MS quantification made it possible to measure the concentrations of each compound using standard reference curves. The limits of detection were 2 nM, 5 nM for the APAP and APAP-GLU; 1 nM, 0.5 nM for the CAF and PARA; 0.3 nM, 0.2 nM, 0.2 nM for the MDZ, 1-OH-MDZ and 4-OH-MDZ; 0.2 nM for the DEXTM, DEX and 3-MM; 0.2 for the OME, OME-SULF and 5-OH-OME; 0.2 nM, 0.1 nM for REP, 1OH-REP and 3OH-REP; and 0.2 nM and 0.5 nM for TOLB and 4OH-TOLB.

Metabolic ratio

Metabolic production over time was calculated as follows:

$$MR = 100x\frac{C(t)}{C_{Po}}$$

in which $C(t)$ is the metabolite concentration in the culture medium at time t and C_{P0} is the initial parent substrate concentration (experimental value).

RTqPCR analysis

Quantitative RT-PCR was performed using the Master Probe Mix (Roche), the Real Time Ready probe system (Roche) and the real time PCR system LC480 (Roche). Briefly, the quality of the total RNA was controlled using the Bioanalyzer 2100 and RNA6000 nanochip kit. cDNA were synthesized from 500 ng of the total RNA with oligodT priming using superscript II (Life technologies) following the recommendations of the vendor. The 16 target genes were studied using the RealTime ready probes from Roche (Table 1). The reference genes were studied using the Sybr green LC480 probes Master. Beta actin (mRNA: NM_001101.3; Forward: 5′GGGTCAGAAGGATTCCTATG3′; Reverse: 5′GGTCTCAAACATGATCTGGG3′; fragment size: 237 bp) and cyclophilin A (PPIA, mRNA: NM_021130; Forward: 5′GGTGACTTCACACGCCATAATG3′; Reverse: 5′ACAAGATGCCAGGACCCGTAT3′; Fragment size: 103 bp) were chosen from a previous pilot study using different housekeeping genes with the Genorm algorithm, allowing us to select these two more stable reference genes in our model. Cq values were extracted with the second derivative maximum method (implemented in the LightCycler® 480 software) and data were analyzed using the ΔCt method. Normalized relative quantities obtained for each sample were used for comparison between the different groups.

Kinetic model for drugs

The drug kinetics in the perfusion system were described by a four-compartment model. This model includes two reservoirs, the hepatic biochip and a compartment representing the tubing between the two reservoirs (Figure 1B). As serum was not used in the experiments, there was no binding of the drugs in the culture medium. Nonspecific binding in the perfusion system was assumed to occur in the tubing. A first order relationship was used for metabolism. These assumptions led to the derivation of a set of first order differential equations:

$$\frac{dQ_{R1}(t)}{dt} = F \times \left(C_T(t) - C_{R1}(t)\right)$$

$$\frac{dQ_{HepB}(t)}{dt} = F \times \left(C_{R1}(t) - C_{HepB}(t)\right) - \sum_X CL_{int,\,in\,vitro,X} \times C_{HepB}(t) - CL_{int,\,in\,vitro,All-Met} \times C_{HepB}(t)$$

Table 1. Sixteen selected target genes studied using Roche RealTime ready probes.

Gene symbol	Assay ID (RTR)	Amplicon size (pb)	Accession ID	Junction exon–exon
CYP1A2	111753	68	ENST00000343932	1–2
HNF4α	102555	61	ENST00000316099	6–7
PGP	105277	150	ENST00000333503	1–2
CAR	111465	86	ENST00000367985	1–2
PXR	137125	90	ENST00000337940	5–6
AHR	102490	82	ENST00000242057	5–6
SULT1A1	138249	106	ENST00000314752	6–7
UGT1A1	138404	76	ENST00000305208	exon 1–2
CYP3A4	135760	78	ENST00000336411	6–7
CYP2E1	110824	73	ENST00000252945	8–9
CYP2C9	111401	121	ENST00000260682	6–7
CYP2C19	111396	78	ENST00000371321	5–6
CYP2C8	111407	79	ENST00000371270	8–9
CYP2D6	135986	74	ENST00000360608	exon 9
CYP2B6	111789	72	ENST00000324071	4–5
OATP	113028	71	ENST00000256958	2–3

$$\frac{dQ_{R2}(t)}{dt} = F \times \left(C_{HepB}(t) - C_{R2}(t)\right) - \frac{dQ_{prev}(t)}{dt}$$

$$\frac{dQ_{T}(t)}{dt} = F \times \left(C_{R2}(t) - C_{T}(t)\right) - \frac{dQ_{Ads}(t)}{dt}$$

where the subscripts *R1, R2, HepB, T* and *X* correspond respectively to the two reservoirs, hepatic biochip and tubing compartments, and the metabolites; F is the flow in the perfusion system (in µL/min); C_i (in pmol/µL) is the concentration in the compartment i; Q_i (in pmol) is the amount in the compartment i; $CL_{int,\ in\ vitro,\ X}$ is the *in vitro* intrinsic clearance that produces the X metabolite (in µL/min/number of hepatocytes in the biochip); $CL_{int,\ in\ vitro,\ All\text{-}X}$ is the *in vitro* intrinsic clearance that is not explained by the production of the measured metabolites (in µL/min/number of hepatocytes in the biochip); k_b (in µL/min/cm^2) and k_u (in min^{-1}.cm^{-2}) are the adsorption and desorption rates for non-specific binding in the tubing; Q_{ads} (in mg) is the quantity adsorbed in the tubing. The latter is given by the following equation:

$$\frac{dQ_{Ads}(t)}{dt} = k_b \times A_{Ads} \times C_T(t) - k_u \times A_{Ads} \times Q_{Ads}(t)$$

where A_{Ads} is the area available for adsorption and is set at 8.7 cm^2 or 9.7 cm^2 in the presence or absence of hepatocytes in the IDCCM box, respectively.

The kinetics of the metabolite(s) were described with a similar model. For one metabolite (subscript *Met*), the model is given by:

$$\frac{dQ_{R1,Met}(t)}{dt} = F \times \left(C_{T,Met}(t) - C_{R1,Met}(t)\right)$$

$$\frac{dQ_{HepB,Met}(t)}{dt} = F \times \left(C_{R1,Met}(t) - C_{HepB,Met}(t)\right) + CL_{int,\ in\ vitro,Met} \times C_{HepB,Met}(t)$$

$$\frac{dQ_{R2,Met}(t)}{dt} = F \times \left(C_{HepB,Met}(t) - C_{R2,Met}(t)\right) - \frac{dQ_{prev,Met}(t)}{dt}$$

$$\frac{dQ_{T,Met}(t)}{dt} = F \times \left(C_{R2,Met}(t) - C_{T,Met}(t)\right)$$

Metabolites were not assumed to be adsorbed in the tubing.

Predicting *in vivo* intrinsic hepatic clearance

The *in vitro* intrinsic clearances expressed per cell estimated from the *in vitro* experiments were scaled to correspond to *in vivo* intrinsic clearance. A scaling factor was applied to express the *in vitro* intrinsic clearances in mL/min/kg of bodyweight. The hepatocellularity was set at 99×10^6 hepatocytes per gram of liver (Barter et al. 2007), and the liver weight to 25 g/kg of bodyweight (Zuegge et al. 2001). Multiplying these two quantities defined the scaling factor (*SF*) for *in vitro/in vivo* extrapolation of the intrinsic clearance.

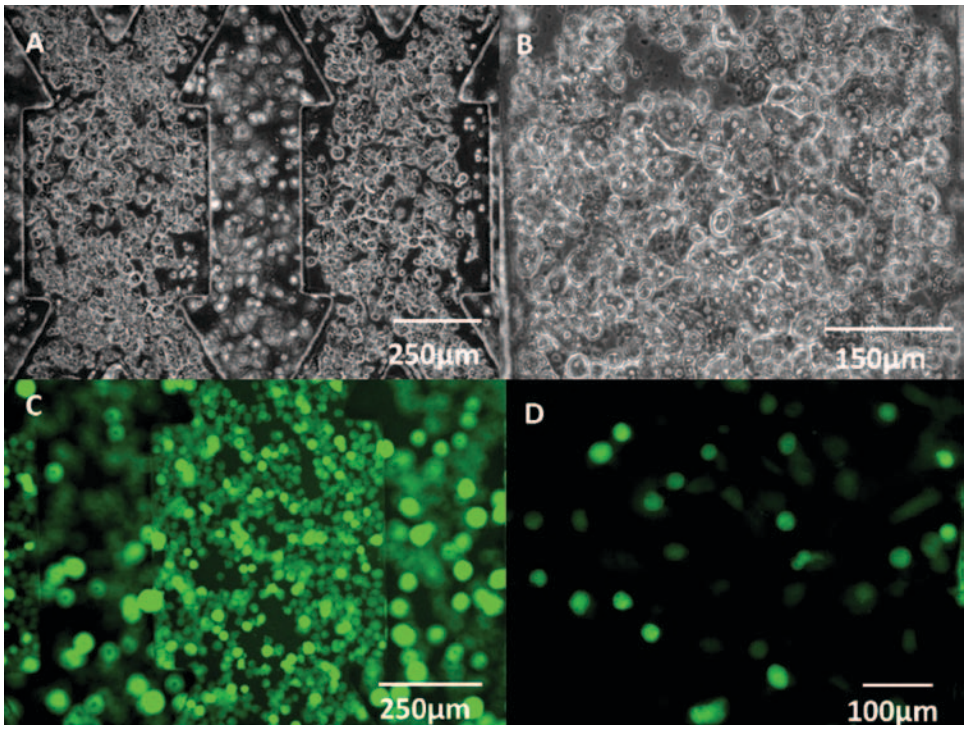

Figure 2. Typical human primary hepatocyte morphologies after 24 h of seeding (A); after 48 h of culture including 24 h of perfusion in the IDCCM box (B); viability detected by calcein AM after 48 h of cultures (C); Fluorescein diacetate staining at the end of the perfusion (D).

Statistical analyses and parameter estimation

Parameters were estimated by fitting the kinetic model to the concentration of drugs in the culture medium. Parameter estimation was performed in a Bayesian framework. Uninformative uniform distributions were used as prior distributions of the parameters. The measurement errors were assumed to be independent and log-normally distributed. Model calibration was performed using the MCSim software (Bois & Maszle 1997). Two independent Monte Carlo Markov Chains (MCMC) were run until convergence was reached. For each parameter, a convergence criterion was used to check convergence at a stable posterior distribution.

Results

Hepatic morphology in the microfluidic biochips

Hepatocyte morphologies after the cell adhesion phase and at the end of the experiments are presented in Figure 2A and 2B. The cells displayed a classical polygonal shape demonstrating successful adhesion in the microfluidic biochip after 24 h of culture without flow. The cell membranes appeared refractive. The cell morphology was maintained after the following 24 h of perfusion. Additional live assays in the biochips illustrated that there was cell viability at the end of the perfusion experiments, as demonstrated by positive calcein AM staining (Figure 2C). In addition, fluorescein diacetate staining performed after 24 h of perfusion illustrated transcellular transport in the microfluidic biochip cultures (Figure 2D). Fluorescein di-acetate is effectively metabolized in hepatocytes, and becomes fluorescein when secreted into bile caniliculi. Although a complete bile network was not achieved, this result highlighted the beginning of functional polarity in the hepatocyte cultures after 48 h of culture (24 h of adhesion and 24 h of perfusion).

Higher hepatic differentiation in dynamic biochips vs static conditions

To illustrate cell functionality and to obtain the status of the level of differentiation by the microfluidic biochip itself, we performed an RTqPCR analysis on untreated cultures (without drug treatments, Table 2). The levels of AHR and HNF4α were reduced by 35% and 60% whereas CAR and PXR fell to 94% and 73%. The levels of the genes related to the cytochromes P450 (CYP1A2, 2B6, 2C8, 2C9, 2C19, 2D6, 2E1, 3A4) were also reduced in the adhered hepatocytes after the seeding period when compared to the post-thawing control. However, as the perfusion was started, the levels of six of the tested genes partially recovered (including HNF4α PXR, CYP1A2, CYP2B6, CYP3A4) when compared to the group of static biochips (Table 2). A continuous reduction in mRNA level was measured at the end of the static experiments leading to a reduction of more than 90% for 15 of the 16 investigated genes. In addition, the RTqPCR analysis revealed that the gene CYP1A2 was the one remaining with the highest expressed values when compared to the post-thawing situation. Finally, the P-gp was found to have upregulated.

Hepatic induction by drugs

We then performed an RTqPCR analysis on the hepatocytes after exposure to the drugs (Table 3). The drugs appeared to act as inductors in our microfluidic configurations. The drugs largely contributed to increasing mRNA levels during microfluidic exposures. Drugs such

Table 2. Comparative expression of CYPs, Phase II enzymes, transporters and mRNA nuclear receptors after hepatocyte thawing, after adhesion in the biochip (24 h) and after the 24 h of perfusion when using the IDCCM box.

	Hepatocytes post-thawing	Plated hepatocytes in biochips (24 h at rest for seeding)	Perfused hepatocytes (24 h of perfusion after the 24 h at rest)	Plated hepatocytes (40 h at rest in biochip)
Gene name	n = 4 samples	n = 3 biochips	n = 7 biochips	n = 3 biochips
HNF4α	100	40 ± 10	85 ± 2	6 ± 1
PXR	100	27 ± 2	54 ± 1	5 ± 1
CAR	100	6 ± 1	9.2 ± 0.2	0.7 ± 0.1
AHR	100	65 ± 20	17 ± 1	10 ± 1
CYP1A2	100	35 ± 5	80 ± 3	6 ± 1
CYP2B6	100	8 ± 2	27 ± 1	1.5 ± 0.2
CYP2C8	100	9 ± 2	4.8 ± 0.2	0.4 ± 0.1
CYP 2C9	100	11 ± 3	11.8 ± 0.3	2.5 ± 0.3
CYP2C19	100	25 ± 5	8.6 ± 0.2	10 ± 1
CYP2D6	100	8 ± 2	3.8 ± 0.1	1.5 ± 0.2
CYP2E1	100	9 ± 1	0.7 ± 0.01	0.6 ± 0.1
CYP3A4	100	35 ± 10	53 ± 2	0.7 ± 0.2
OATP2	100	35 ± 10	98 ± 2	3 ± 0.5
Pgp	100	200 ± 60	74 ± 4	74 ± 8
SULT1A1	100	12 ± 1	4.7 ± 0.1	2 ± 1
UGT1A1	100	30 ± 10	7.5 ± 0.2	6 ± 1

After 24 h of adhesion, the culture medium (1 mL/biochip) was perfused at a flow rate of 25 µL/min for 24 h. Results are expressed as a % compared to the levels in the hepatocytes after thawing. The results were obtained from two independent experiments but the same couple of donors.

Table 3. Comparative expression of CYPs, Phase II enzymes, transporters and mRNA nuclear receptors after hepatocyte thawing, after adhesion in the biochip (24 h) and after the 24 h of perfusion with treatment when using the IDCCM box.

	Post-thawing	Post-adhesion	Control	APAP	CAF	DEXTM	MDZ	OME	TOLB	REP
HNF4α	100	40 ± 10	85 ± 2	228	77	360	102	200	291	94
PXR	100	27 ± 2	54 ± 1	210	88	228	110	154	191	49
CAR	100	6 ± 1	9.2 ± 0.2	185	52	115	98	214	203	8
AHR	100	65 ± 20	17 ± 1	49	44	437	147	210	30	21
CYP1A2	100	35 ± 5	80 ± 3	406	155	276	172	188	110	70
CYP2B6	100	8 ± 2	27 ± 1	169	90	269	49	270	330	31
CYP2C8	100	9 ± 2	4.8 ± 0.2	54	90	118	41	188	140	4
CYP2C9	100	11 ± 3	11.8 ± 0.3	119	83	139	64	177	216	12
CYP2C19	100	25 ± 5	8.6 ± 0.2	41	100	404	72	170	111	9
CYP2D6	100	8 ± 2	3.8 ± 0.1	32	91	54	68	173	62	3
CYP2E1	100	9 ± 1	0.7 ± 0.01	9	83	84	77	160	11	1
CYP3A4	100	35 ± 10	53 ± 2	110	78	265	75	225	92	64
OATP2	100	35 ± 10	98 ± 2	259	80	150	130	180	124	106
Pgp	100	200 ± 60	74 ± 4	25	112	58	34	197	110	103
SULT1A1	100	12 ± 1	4.7 ± 0.1	30	97	57	77	155	41	5
UGT1A1	100	30 ± 10	7.5 ± 0.2	28	128	360	78	153	85	8

Results are expressed as a % compared to the levels in the hepatocytes after thawing (n = 4). The drug results were obtained from a pool of two biochips for each case. Controls (n = 7 biochips) and post-adhesion data (n = 3 biochips) come from Table 2.

Table 4. Substrates and metabolites investigated in the IDCCM box after 24 h of perfusion.

Substrates	Metabolites	Enzymes	Activity analyzed by MS
Acetaminophen (APAP)	Acetaminophen Glucuronide (APAP-GLU)	UGT1A1	Screened for and not detected
Caffeine (CAF)	Paraxanthine (PARA)	CYP1A2	Detected
Dextromethorphan (DEXTM)	Dextrorphan (DEX)	CYP2D6	Detected
	3-methoxymorphinan (3-MM)	CYP3A4	Screened for and not detected
Midazolam (MDZ)	1-hydroxymidazolam (1-OH-MDZ)	CYP3A4	Detected
	4-hydroxymidazolam (4-OH-MDZ)	CYP3A4	Screened for and not detected
Omeprazole (OME)	5-hydroxyomeprazole (5-OH-OME)	CYP2C19	Detected
	Omeprazole Sulfone (OME-SULF)	CYP3A4	Detected
Tolbutamide (TOLB)	4-hydroxytolbutamide (4-OH-TOLB)	CYP 2C9	Detected
Repaglinide (REP)	3-hydroxyrepaglinide (3-OH-REP)	CYP 2C8	Screened for and not detected
	Hydroxyrepaglinide (OH-REP)	CYP 2C8	Detected

as DEXTM, OME and TOLB induced transcription factor HNF4α. The dependent membrane receptors (PXR, CAR) and related cytochromes (CYP3A4, CYP2B6, CYP2C8, CYP2C9 and CYP2C19) were also induced at values greater than those found in the post-thawing control. In addition, REP, a substrate of cell transporters, played an important part in allowing the recovery of the post-thawing levels of OATP2 and Pgp, both involved in its excretion. All drugs improved the level of CYP1A2. AHR and the related genes (UGT1A, SULT1A and CYP1A2) were highly upregulated by DEXTM and OME during the microfluidic cultures.

Metabolism analysis

To confirm whether or not the hepatic functions were maintained in the liver biochip of the IDCCM box, we performed drug metabolism experiments. To do so, we analyzed 7 substrates of the main CYPs and quantified their metabolite production (Table 4). Due to the features of our IDCCM device, including a silicone biochip, polycarbonate bow and PTFE tubes, we also investigated

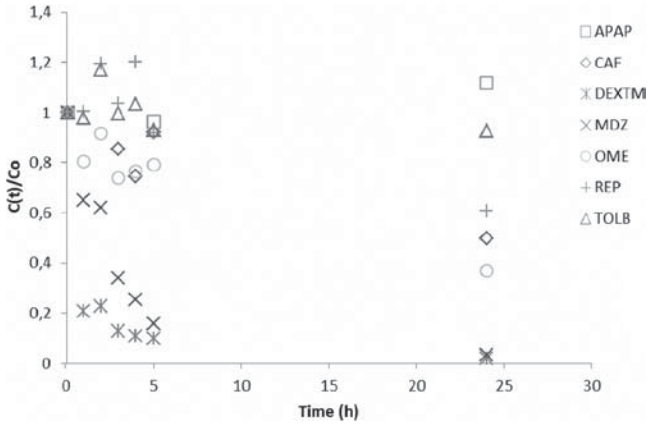

Figure 3. Quantification of adsorption in the IDCCM box and fluid circuit of the substrates with PTFE tubes.

substrate adsorption. The non-specific binding experiments showed that substrates were adsorbed in the perfusion circuit and that the adsorption differed greatly between the drugs (Figure 3). After 24 h of perfusion, adsorption on circuit components was almost complete

Table 5. Estimated parameters for the kinetic model and comparison with literature data using cryopreserved human hepatocytes.

Drug	k_b (10^{-3} µL/min/cm^2)	k_{ub} (µL^{-1} cm^{-2})	Biochip: $CL_{int,\ in\ vitro}$ (µL/min/10^6 cells)	Predicted from Biochip: $CL_{int,\ in\ vivo}$ (mL/min/kg of bw)	Literature data: $CL_{int,\ in\ vitro}$ (µL/min/10^6 cells)	Literature data: *Predicted* $CL_{int,\ in\ vivo}$ (mL/min/kg of bw)	Literature data: *Observed* $CL_{int,\ in\ vivo}$ (mL/min/kg of bw)	Biochip fold under prediction
Omeprazole	0.161 ± 0.003	1.06 ± 0.03						
X = 5-hydroxy			0.019 ± 0.011	0.047 ± 0.027				
X = sulfone			0.014 ± 0.005	0.036 ± 0.012				
All-X			0.065 ± 0.069	0.163 ± 0.170				
All			0.098 ± 0.08	0.246 ± 0.3	1.7[a]	4.5[a]	12[a]	48
Midazolam	0.032 ± 0.001	1.71 ± 0.03						
X = 1-hydroxy			0.034 ± 0.005	0.085 ± 0.013	40[b]			
All-X			0.282 ± 0.051	0.711 ± 0.126				
All			0.316 ± 0.52	0.793 ± 0.13	7–14[a,c,d]	37[a]	9.9[a]	12
Dextromethorphan	0.033 ± 0.001	3.42 ± 0.05						
X = dextorphan			0.188 ± 0.019	0.475 ± 0.048	1.6–63[e]			
All-X			0.270 ± 0.280	0.68 ± 0.693				
All			0.458 ± 0.3	1.155 ± 0.7	8–15[a]	20[a]	8.6[a]	7.4
Repaglinide	0.879 ± 0.042	0.49 ± 0.03						
X = Hydroxy			0.018 ± 0.005	0.046 ± 0.013				
All-X			0.148 ± 0.003	0.372 ± 0.008				
All			0.166 ± 0.01	0.418 ± 0.14	119[f]	0.74[f]–6.8[f]	7.8[f]	18
Tolbutamide	1.200 ± 0.077	0.30 ± 0.02						
X = 4-hydroxy			0.028 ± 0.004	0.07 ± 0.011	0.06[e]			
All-X			0.012 ± 0.009	0.03 ± 0.023				
All			0.04 ± 0.013	0.1 ± 0.034	1.6[c,d]	0.38[e]	4.9[e]	49

"All" denotes the global parent drug clearance; "X" denotes the metabolite clearance measured in our experiments, "All-X" denotes the portion of the clearance resulting from other metabolites (adsorption of parent drug being already taken into account in the model).
[a]McGinnity et al. (2004).
[b]Hallifax et al. (2004).
[c]Benet et al. (1996).
[d]Lau et al. (2002).
[e]Brown et al. (2007).
[f]Jones et al. (2012).

for midazolam and dextromethorphan (close to 100%). For the other drugs, adsorption ranged from 40% for repaglinide to about 60% for tolbutamide and omeprazole after 24 h of perfusion. The model without metabolism (i.e., $CL_{int,\ in\ vitro}$ set at 0) was fitted to the concentration of drugs in the culture medium. Table 5 sums up the parameter estimates for adsorption/desorption k_b and k_{ub} (defined as the ratio k_u/k_b) for each drug. Metabolite detection in the IDCCM box reservoir illustrated that CYP remained functional in our culture configuration. Indeed, we were able to detect the transformation of caffeine into paraxanthine (CYP1A2), of midazolam into 1OH-midazolam (CYP3A4), of dextromethorphan into dextorphan (CYP2D6), of omeprazole into 5 OH-omeprazole and omeprazole sulfone (CYP2C19 and CYP3A4), of tolbutamide into OH-tolbutamide (CYP2C9), of repaglinide into OH-repaglinide (CYP2C8). Although the mass spectrometer was tuned for 4OH-midazolam, 3-methoxymorphinan, APAP-GLU and 3-OH-repaglinide, we were not able to detect these compounds in the respective metabolism experiments. In addition, the time lapse analysis revealed that the rate of metabolite production increased with time for the CYP3A4, CYP2C8, CYP2C9 and CYP2C19 substrates (Figure 4). On the contrary, the rate of metabolite production for CYP1A2 and CYP2D6 substrates remained stable with time (Figure 4).

Finally, the mean production rate for the detected metabolites over the 24 h of cultures is presented in Figure 5. Paraxanthine (CYP1A2) was found to have the lowest production rate (14 ± 6 pmol/min/10^6 cells) whereas the fastest rate (187 ± 35 pmol/min/10^6 cells) was found for 4-OH-tolbutamide (CYP2C9). Two metabolites, 1OH-midazolam and omeprazole-sulfone, both produced by CYP3A4, reached production rates close to 50 pmol/min/10^6 cells in our biochips.

Estimating the *in vitro* intrinsic clearance in the microfluidic biochip

We observed that the drug was cleared from the culture medium at a higher rate when hepatocytes were incubated in the biochip than in the non-specific binding experiments. This demonstrated a metabolic activity of primary hepatocytes in the microfluidic biochips despite

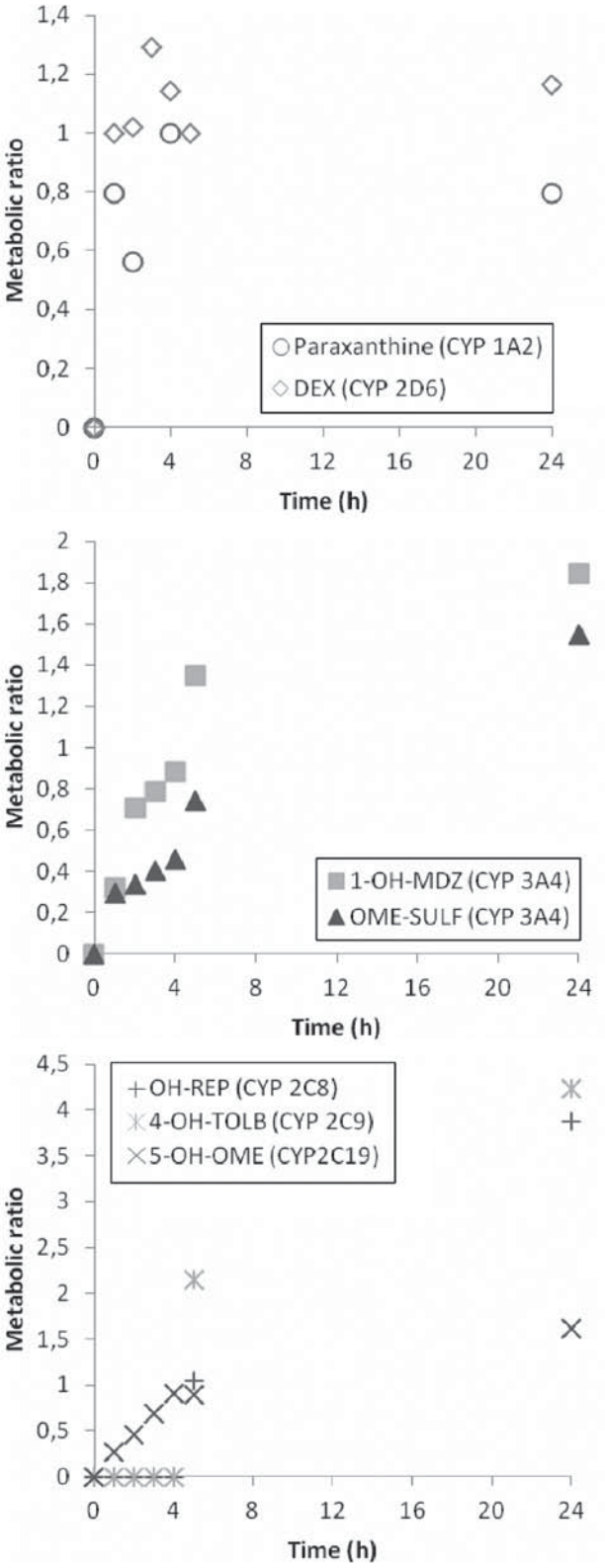

Figure 4. Metabolic ratio of metabolite appearance during microfluidic cultures.

the adsorption phenomena. Figure 6 presents the experimental data on the depletion and apparition of the different substrates with the superimposition of the kinetic profiles estimated with the model. The modelled profiles take adsorption into account. We observe that the model was able to reproduce the drugs' kinetics. Table 5 sums up the estimated *in vitro* intrinsic clearances in the biochips. The values of the biochip intrinsic clearances for midazolam, tolbutamide, omeprazole, repaglinide and dextromethorphan were 0.326; 0.04; 0.098; 0.166 and 0.458 μL/min/10^6 cells respectively. The estimated *in vitro* intrinsic clearances obtained from the biochips were then transposed to predicted *in vivo* intrinsic hepatic clearances (Table 5).

Discussion

Identifying pertinent *in vitro* screening models for predicting an *in vivo* physiological hepatic situation is of great importance. Apart from the model used, the liver microfluidic biochip makes continuous dynamical hepatocyte cultures possible. Furthermore, the successful integration of microfluidic biochips into conventional well plate formats leads to a "physical" support for the biochip to be commercially available in automated and robotic devices. In this context, our design makes possible the parallelized culture of 12 biochips. In this study, we showed that we were able to cultivate human cryopreserved hepatocytes in those parallelized devices. In addition, the results showed that the hepatocytes remained functional as illustrated by the metabolism study.

The RTqPCR analysis revealed that the levels of the genes responsible for drug metabolism were reduced after the adhesion phase. This critical point has been widely observed in numerous plated hepatocyte cultures (Guillouzo et al. 1997, Guillouzo 1998; Hewitt et al. 2001, 2007). In order to limit this reduction it is necessary to develop powerful liver tissue engineered cultures. Improvements can be proposed based on the implementation of a specifically optimized extracellular matrix for liver tissue cultures (such as matrigel coating) and co-culture models (such as with hepatocytes and non-parenchymal cells). Novik et al. 2010 have shown that these implementations play a part in enhancing various CYP P450 expressions in Petri cultures and can be successfully transferred to microfluidic biochip cultures. In our study, once the perfusion had started, reduction of the various CYP expressions ended and their levels were maintained. The effect of a microfluidic environment and of flow rate in maintaining CYP activity has been already reported in the literature (Tilles et al. 2001, Sivaraman et al. 2005; Park et al. 2005; Novik et al. 2010) and appeared consistent with our results. This finding also appeared consistent with our previous study using cell lines in which various cytochrome P450 were upregulated in our microfluidic biochip cultures (Prot et al. 2011a). Although we did not perform specific induction assays (using rifampicin, for instance, for CYP3A4) we demonstrated the inducibility of the hepatocytes in our biochips by the tested drugs which appeared consistent with the literature (Tompkins & Wallace 2007, Pelkonen et al. 2008).

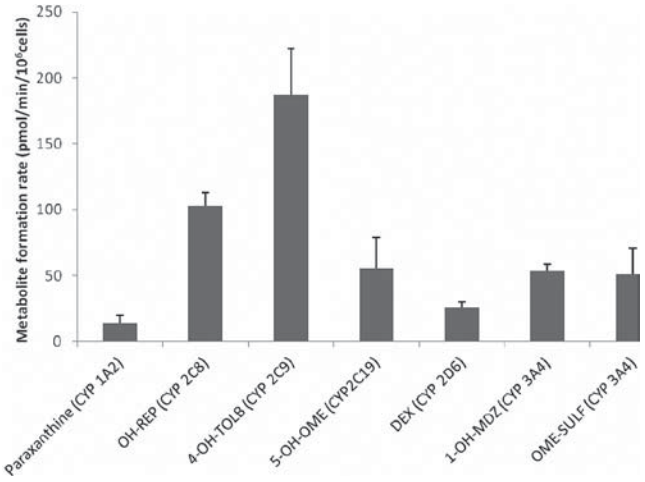

Figure 5. Metabolite production rates in the microfluidic cultures after 24 h of perfusion.

In addition, the RTqPCR analysis showed that the level of the P-gp and OATP2 genes was upregulated in our culture configuration. P-gp is involved in drug transport and is located at the interface between hepatocytes and bile ducts acting to efflux drugs from the body. Combined with the positive fluorescein diacetate staining, these results demonstrated a developing polarity in the hepatocytes cultivated in the biochips. These observations can be taken as evidence of cellular uptake and probable canalicular secretion of the dye (Barth & Schwarz 1982). Interestingly, the Pgp gene is involved in the multidrug resistance which is reported to limit xenobiotic disposition *in vivo* (Paine et al. 2008). Extensive future investigations will thus be required to decide whether our culture conditions can reproduce *in vitro* this limitation observed *in vivo*.

In the metabolism analysis, we were able to metabolize 6 of the 7 tested CYP substrates (caffeine, midazolam, omeprazole, tolbutamide, dextromethorphan, repaglinide). Consistently with other liver microfluidic biochips (Novik et al. 2010), we achieved functional cytochromes such as CYP1A2, CYP3A4, CYP2C8, CYP2C9 and CYP2C19. However, the difference in the absolute values of metabolite production between various biochips or other *in vitro* data in the literature can be attributed to several parameters related to the donors, hepatocyte extraction, metabolite adsorption in the circuit, biochip design or to the culture process itself, drug concentration (V_{max} studies for instance). Nevertheless, when compared to plated cultures, the microfluidic cultures increased most of the production rates for the investigated drug metabolisms (Novik et al. 2010; Prot et al. 2011c). When compared to the metabolism in suspension using human cryopreserved hepatocytes (see Hallifax et al. 2004 for midazolam), the metabolite formation rate in biochips appeared slower. The difference can be attributed to several factors. The first is the reduction in mRNA levels during the adhesion phase which may lead to weaker metabolism capability in biochips when compared to suspensions. The second explanation may be related to transporters and active uptake/efflux from our hepatocyte cultures. In suspensions, efflux transporters are not active due to the loss of cell polarity and redistribution of canalicular membranes (Groothuis & Meijer 1996); therefore, the compound remained in the cell, leading to higher metabolism (Griffin & Houston 2005). In addition, a third consideration is the adsorption of the metabolites in the perfusion circuit (as illustrated in our previous work; Prot et al. 2011c) that reduced the detectable quantities. This hypothesis is unlikely except for midazolam, dextrometorphan and apolar metabolites. However, when compared to the literature using suspensions or plated hepatocytes, we were able to perform the analysis over 24 h of culture (unlike short term cultures carried out over 2 h with sampling every 10 min). Finally, the biotransformation levels in the biochips were not obtained at the substrate concentration corresponding to the V_{max} value which normally leads to the maximal disappearance rate for the drugs. This shows that the V_{max}/Km couple values must be investigated in our next development in order to complete the performance analysis of our biochips.

Finally, Chao et al. (2009) used biochips similar to those of Novik et al. (2010) to investigate drug clearances. They demonstrated that biochip analysis can be used to extract intrinsic *in vitro* hepatic clearances and to predict *in vivo* situations (especially concerning imipramine, buspirone and sildenafil). Their results illustrated a higher predictability in biochips when compared to plated hepatocytes cultures. Our biochip did not reach such performance levels. In the present work, we have modelled the *in vitro* intrinsic clearance and used it to predict an *in vivo* intrinsic clearance. When compared to other *in vitro* models using cryopreserved human hepatocytes (plated or sandwiched cultures), our intrinsic clearances appeared weaker (Table 5). Although the microfluidic cultures and drugs induced mRNA levels related to drug metabolism genes, the values of the intrinsic predicted clearances were lower than those observed *in vivo*. Even if we modelled the adsorption, the lowest or most moderately adsorbed molecules (such as tolbutamide or omeprazole) did not reach the values reported in the literature. This might be due to the effects described above (multi-drug resistance enzyme activities, concentrations leading to V_{max} values, etc.) that were not taken into account. In addition, we have not yet taken into account the compounds binding to the culture medium element (such as to the albumin produced by the hepatocytes) that reduced drug metabolism.

Conclusion

In this study, we have presented the perfusion culture for human cryopreserved hepatocytes in parallelized microfluidic biochips. The results have shown that the hepatocytes were viable and functional after 48 h of culture including 24 h of adhesion and 24 h of perfusion in the IDCCM configurations. The RTqPCR

analysis revealed that the adhesion step played a part in reducing the mRNA level of the gene involved in drug metabolism. This reduction was reduced once the microfluidic perfusion started in the biochips leading to a partial recovery of the post-thawing situations. The CYP functionality was confirmed by the metabolism of midazolam, caffeine, dextromethorphan, tolbutamide, omeprazole, repaglinide. The kinetic model based on the substrate clearances was able to reproduce the experimental data. The model made it possible to extract and predict *in vitro* and *in vivo* intrinsic hepatic clearances. However, the predicted clearance did not reach the values observed *in vivo*. These findings illustrate the potential parallelized microfluidic cultures have for reproducing hepatic tissue functions. However several improvements concerning the biochips and circuit materials, as well as the drug-free fraction analysis, must be made before we can achieve more functional tools for drug screening and metabolism applications.

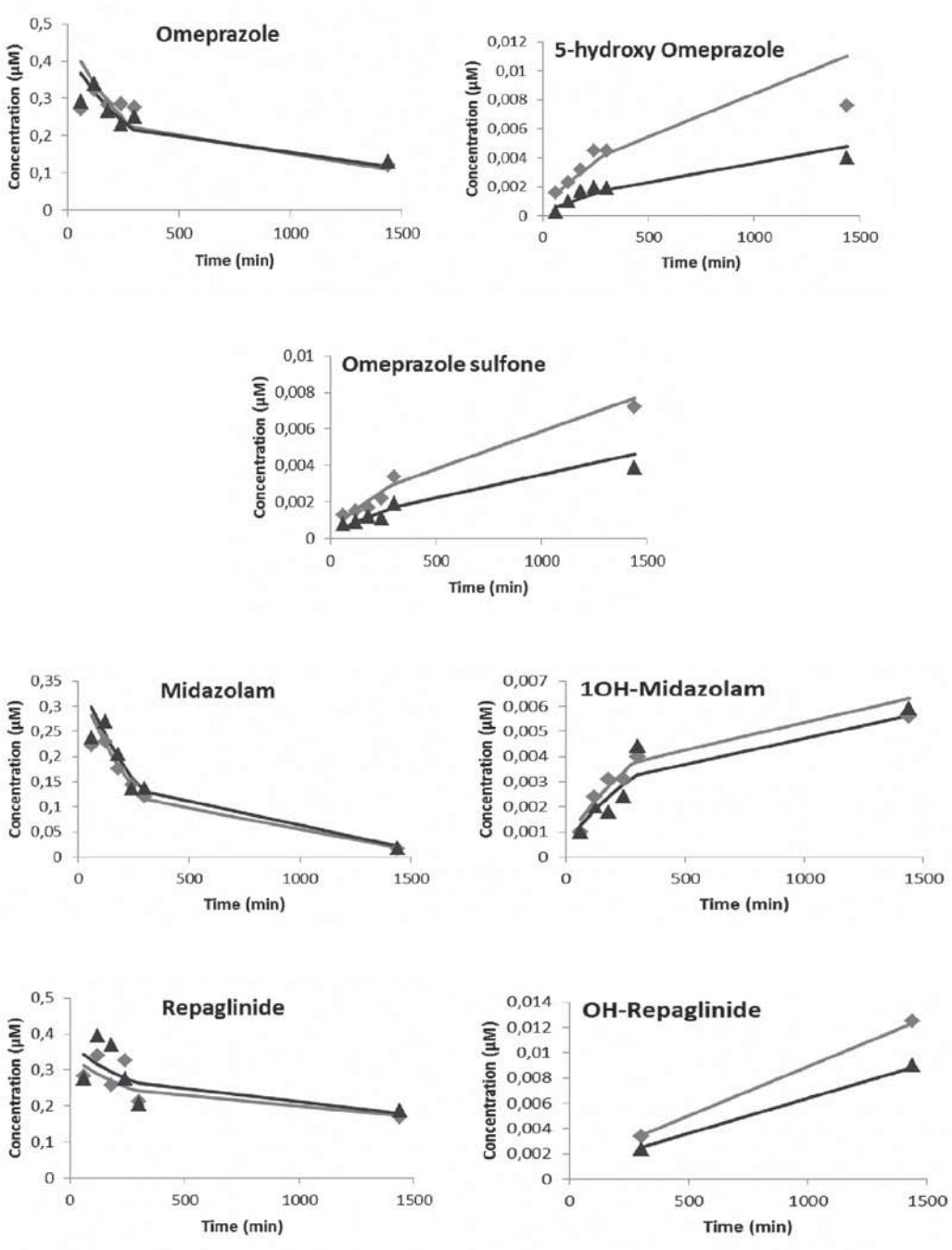

Figure 6. Kinetics of drugs and metabolites in the hepatic biochips during metabolism experiments. The symbols correspond to the experimental concentrations of the molecules measured from mass spectrometry analysis. For each molecule, the experimental points come from two independent biochips. The solid lines are the model fit to the measured concentrations taking into account the adsorption phenomena.

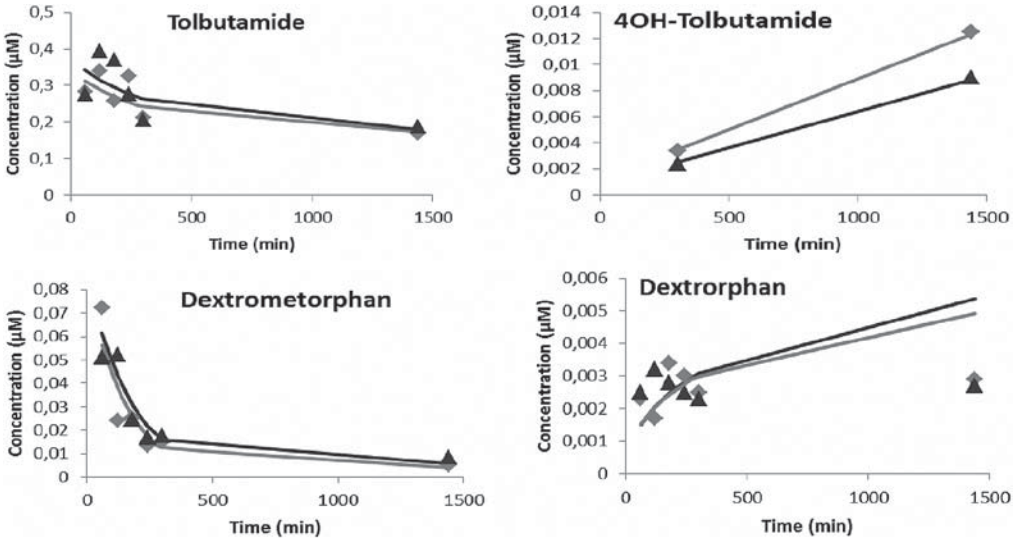

Figure 6. (Continued).

Acknowledgments

The authors thank Laurent Griscom from UMR 8089 SATIE Biomis, ENS de Cachan who manufactured the master mold used in this study.

Declaration of interest

This work was supported by the "fondation pour la recherche et l'innovation" at the Université de Technologie de Compiègne and by the CNRS. Régis Baudoin received a grant from the CNRS via a research valorization program. Jean Matthieu Prot received a grant from the post-grenelle 189 project "Activism".

References

Barter ZE, Bayliss MK, Beaune PH, Boobis AR, Carlile DJ, Edwards RJ, Houston JB, Lake BG, Lipscomb JC, Pelkonen OR, Tucker GT, Rostami-Hodjegan A. (2007). Scaling factors for the extrapolation of *in vivo* metabolic drug clearance from *in vitro* data: Reaching a consensus on values of human microsomal protein and hepatocellularity per gram of liver. Curr Drug Metab 8:33–45.

Benet LZ, Øie S, Schwartz JB. (1996). Goodman and Gilman's: The pharmacological basis of therapeutics. Gilman AG, Hardman JG, Limbard LE, Molinoff PB, Ruddon RW, eds. 9th ed. New York: McGraw Hill Book Company.

Barth CA, Schwarz LR. (1982). Transcellular transport of fluorescein in hepatocyte monolayers: Evidence for functional polarity of cells in culture. Proc Natl Acad Sci USA 79:4985–4987.

Baudoin R, Griscom L, Prot JM, Legallais C, Leclerc E. (2011). Behavior of HepG2/C3A cell cultures in a microfluidic bioreactor. Biochem Eng J 53:172–181.

Baudoin R, Liberto G, Legallais C, Leclerc E. (in press). Development of a culture box for parallelized microfluidic biochips for xenobiotic toxicity applications. Sensors and Actuators B.

Bhogal N, Grindon C, Combes R, Balls M. (2005). Toxicity testing: Creating a revolution based on new technologies. Trends Biotechnol 23:299–307.

Blaauboer BJ, Andersen ME. (2007). The need for a new toxicity testing and risk analysis paradigm to implement REACH or any other large scale testing initiative. Arch Toxicol 81:385–387.

Bois F, Maszle D. (1997). MCSim: A simulation program. J Stat Software 2:1–60.

Brown HS, Griffin M, Houston JB. (2007). Evaluation of cryopreserved human hepatocytes as an alternative *in vitro* system to microsomes for the prediction of metabolic clearance. Drug Metab Dispos 35:293–301.

Chao P, Maguire T, Novik E, Cheng KC, Yarmush ML. (2009). Evaluation of a microfluidic based cell culture platform with primary human hepatocytes for the prediction of hepatic clearance in human. Biochem Pharmacol 78:625–632.

Cheng S, Prot JM, Leclerc E, Bois FY. (2012). Zonation-related pathways in human hepatocellular carcinoma cells in dynamic vs. static culture microenvironments. BMC Genomic 13:54.

Greim H, Arand M, Autrup H, Bolt HM, Bridges J, Dybing E, Glomot R, Foa V, Schulte-Hermann R. (2006). Toxicological comments to the discussion about REACH. Arch Toxicol 80:121–124.

Griffin SJ, Houston JB. (2005). Prediction of *in vitro* intrinsic clearance from hepatocytes: Comparison of suspensions and monolayer cultures. Drug Metab Dispos 33:115–120.

Griffith LG, Naughton G. (2002). Tissue engineering–current challenges and expanding opportunities. Science 295:1009–1014.

Groothuis GM, Meijer DK. (1996). Drug traffic in the hepatobiliary system. J Hepatol 24 Suppl 1:3–28.

Guillouzo A. (1998). Liver cell models in *in vitro* toxicology. Environ Health Perspect 106 Suppl 2:511–532.

Guillouzo A, Morel F, Langouët S, Maheo K, Rissel M. (1997). Use of hepatocyte cultures for the study of hepatotoxic compounds. J Hepatol 26 Suppl 2:73–80.

Hallifax D, Rawden H, Hakooz N, Houston B. (2004). Prediction of metabolic clearance using cryopreserved human hepatocytes: Kinetic characteristic for five benzodiazepines. Drug Metab Dispos 33:115–120.

Hartung T, Rovida C. (2009). Chemical regulators have overreached. Nature 460:1080–1081.

Hewitt NJ, Bühring KU, Dasenbrock J, Haunschild J, Ladstetter B, Utesch D. (2001). Studies comparing *in vivo*:*in vitro* metabolism of three pharmaceutical compounds in rat, dog, monkey, and human using cryopreserved hepatocytes, microsomes, and collagen gel immobilized hepatocyte cultures. Drug Metab Dispos 29:1042–1050.

Hewitt NJ, Lechón MJ, Houston JB, Hallifax D, Brown HS, Maurel P, Kenna JG, Gustavsson L, Lohmann C, Skonberg C, Guillouzo A, Tuschl G, Li AP, LeCluyse E, Groothuis GM, Hengstler JG. (2007). Primary hepatocytes: Current understanding of the regulation of metabolic enzymes and transporter proteins, and pharmaceutical practice for the use of hepatocytes in metabolism, enzyme

induction, transporter, clearance, and hepatotoxicity studies. Drug Metab Rev 39:159–234.

Jones H, Barton H, Lai Y, Bi Y, Kimoto E, Kempshall S, Tate S, El-Kattan A, Houston B, Galetin A, Fenner K. (2012). Mechanistic pharmacokinetic modeling for the prediction of transporter-mediated disposition in human from sandwich culture human hepatocyte data. doi:10.1124/dmd.111.042994

Lau YY, Sapidou E, Cui X, White RE, Cheng KC. (2002). Development of a novel *in vitro* model to predict hepatic clearance using fresh, cryopreserved, and sandwich-cultured hepatocytes. Drug Metab Dispos 30:1446–1454.

McGinnity DF, Soars MG, Urbanowicz RA, Riley RJ. (2004). Evaluation of fresh and cryopreserved hepatocytes as *in vitro* drug metabolism tools for the prediction of metabolic clearance. Drug Metab Dispos 32:1247–1253.

Novik E, Maguire TJ, Chao P, Cheng KC, Yarmush ML. (2010). A microfluidic hepatic coculture platform for cell-based drug metabolism studies. Biochem Pharmacol 79:1036–1044.

Ouattara DA, Prot JM, Bunescu A, Dumas ME, Elena-Herrmann B, Leclerc E, Brochot C. (2012). Metabolomics-on-a-chip and metabolic flux analysis for label-free modeling of the internal metabolism of HepG2/C3A cells. Mol Biosyst 8:1908–1920.

Paine SW, Parker AJ, Gardiner P, Webborn PJ, Riley RJ. (2008). Prediction of the pharmacokinetics of atorvastatin, cerivastatin, and indomethacin using kinetic models applied to isolated rat hepatocytes. Drug Metab Dispos 36:1365–1374.

Park J, Berthiaume F, Toner M, Yarmush ML, Tilles AW. (2005). Microfabricated grooved substrates as platforms for bioartificial liver reactors. Biotechnol Bioeng 90:632–644.

Pelkonen O, Turpeinen M, Hakkola J, Honkakoski P, Hukkanen J, Raunio H. (2008). Inhibition and induction of human cytochrome P450 enzymes: Current status. Arch Toxicol 82:667–715.

Powers MJ, Janigian DM, Wack KE, Baker CS, Beer Stolz D, Griffith LG. (2002). Functional behavior of primary rat liver cells in a three-dimensional perfused microarray bioreactor. Tissue Eng 8:499–513.

Prot JM, Aninat C, Griscom L, Razan F, Brochot C, Guillouzo CG, Legallais C, Corlu A, Leclerc E. (2011a). Improvement of HepG2/C3a cell functions in a microfluidic biochip. Biotechnol Bioeng 108:1704–1715.

Prot JM, Briffaut AS, Letourneur F, Chafey P, Merlier F, Grandvalet Y, Legallais C, Leclerc E. (2011b). Integrated proteomic and transcriptomic investigation of the acetaminophen toxicity in liver microfluidic biochip. PLoS ONE 6:e21268.

Prot JM, Videau O, Brochot C, Legallais C, Bénech H, Leclerc E. (2011c). A cocktail of metabolic probes demonstrates the relevance of primary human hepatocyte cultures in a microfluidic biochip for pharmaceutical drug screening. Int J Pharm 408:67–75.

Sivaraman A, Leach JK, Townsend S, Iida T, Hogan BJ, Stolz DB, Fry R, Samson LD, Tannenbaum SR, Griffith LG. (2005). A microscale *in vitro* physiological model of the liver: Predictive screens for drug metabolism and enzyme induction. Curr Drug Metab 6:569–591.

Shintu L, Baudoin R, Navratil V, Prot JM, Pontoizeau C, Defernez M, Blaise BJ, Domange C, Péry AR, Toulhoat P, Legallais C, Brochot C, Leclerc E, Dumas ME. (2012). Metabolomics-on-a-chip and predictive systems toxicology in microfluidic bioartificial organs. Anal Chem 84:1840–1848.

Tilles AW, Baskaran H, Roy P, Yarmush ML, Toner M. (2001). Effects of oxygenation and flow on the viability and function of rat hepatocytes cocultured in a microchannel flat-plate bioreactor. Biotechnol Bioeng 73:379–389.

Tompkins LM, Wallace AD. (2007). Mechanisms of cytochrome P450 induction. J Biochem Mol Toxicol 21:176–181.

Videau O, Delaforge M, Levi M, Thevenot E, Gal O, Becquemont L, Beaune P, Benech H. (2010). Biochemical and analytical development of the CIME cocktail for drug fate assessment in humans. Rapid Commun Mass Spectrom 24:2407–2419. Available at: http://dx.doi.org/10.1002/rcm.4641.

Zhang S, Tong W, Zheng B, Susanto TA, Xia L, Zhang C, Ananthanarayanan A, Tuo X, Sakban RB, Jia R, Iliescu C, Chai KH, McMillian M, Shen S, Leo H, Yu H. (2011). A robust high-throughput sandwich cell-based drug screening platform. Biomaterials 32:1229–1241.

Zuegge J, Schneider G, Coassolo P, Lavé T. (2001). Prediction of hepatic metabolic clearance: Comparison and assessment of prediction models. Clin Pharmacokinet 40:553–563.